Fuel 353 (2023) 129182

Contents lists available at ScienceDirect

Fuel

journal homepage: www.elsevier.com/locate/fuel

Full Length Article

Self-Acceleration and global pulsation of unstable laminar Hydrogen-Air flames

Yu Xie [a], Mohamed Elsayed Morsy [a,b], Junfeng Yang [a,*]

[a] School of Mechanical Engineering, University of Leeds, Leeds LS2 9JT, United Kingdom
[b] Faculty of Engineering at El-Mattaria, Helwan University, Cairo 11718, Egypt

ARTICLE INFO

Keywords:
Spherically expanding flame
Self-similarity
Acceleration exponent
Global pulsation

ABSTRACT

The self-acceleration and global pulsation of spherically expanding laminar hydrogen-air flames were studied in a spherical explosion vessel, over a wide range of equivalence ratios (0.4–2.0), initial temperatures (300–400 K), and initial pressures (0.1–0.7 MPa). Comprehensive quantitative data on the self-acceleration propagation of unstable laminar hydrogen-air flames were obtained. The results show that the self-similarity appears after the onset of instability, and the previous assertion of acceleration exponent $\alpha = 1.5$ is not valid for hydrogen-air flames. The derived values of α for such flames vary from 1.125 and 1.39 in the present work. For the self-accelerating flame, the temporal evolution of the flame radius is described by $r_u = At^{\alpha}$, and temporal flame propagation speed is described by $S_n = A\alpha t^{\alpha-1}$. A modified theoretical expression of the constant A is proposed and validated against the present experimentally derived results. The acceleration phase after flame instability presents a global pulsating acceleration pattern. The frequency of global pulsation rises as the pressure or temperature of the flame increases. A pulsing flame speed equation can be used to reliably estimate flame speed after the onset of cellular instability. Self-acceleration observed in small laboratory explosions can serve as a predictive indicator for flame behaviour on a larger atmospheric scale.

1. Introduction

Flame instabilities induced by either the Darrieus-Landau (D-L), or the thermal-diffusional (T-D) instability lead to wrinkling of the smooth laminar flame front, and consequently increase the total flame surface area and through it the global flame propagation speed. It has become widely accepted that spherically expanding laminar flame, propagating at constant pressure, is subjected to a transition from stable smooth to cross-cracking, and eventually, a coherent cellular structure covering the entire flame surface due to D-L and T-D instabilities. The developed cellular structures are accompanied by an increase in flame speed, as a result of the rapid increase in flame surface area; this phenomenon is referred to as self-acceleration [1–2]. The cells continue to grow and divide during flame growth, and develop a self-similar fractal character of the flame front, which is the so-called fractal phenomenon [3–4]. The corresponding fractal theory has been developed to study the small- [5–6] and large- [7–9] scale flame propagation.

For the self-accelerating flame, the history of the flame radius after the onset of flame instability is described by the following power-law [3]:

$$r_u = At^{\alpha} \tag{1}$$

where r_u is the flame cold front radius, t is the time after spark ignition, A is the empirical constant, α is the acceleration exponent. It is worth noting that instead of the radius, the fundamental theory on self-similar propagation is applied to the speed, then the acceleration exponent, A and α can be derived through flame speed correlation [1]:

$$S_n = \frac{dr_u}{dt} = A\alpha t^{\alpha-1} = A^{\frac{1}{\alpha}}\alpha(r_u)^{\frac{\alpha-1}{\alpha}}\, r_u^{\frac{\alpha-1}{\alpha}} = r_u^{d} \tag{2}$$

where d is the fractal excess, expressed as: $d = (\alpha - 1)/\alpha$. This relationship is derived directly from the fractal description of flame propagation. Besides, the wrinkled flame front can be considered as a fractal surface with the total flame surface area. The fractal excess, d, is commonly used as an indicative factor, to assess whether the flame exhibits self-similarity ($0 < d < 1/3$, correspondingly, $1 < \alpha < 3/2$) or reach self-turbulization ($1/3 < d$, correspondingly, $3/2 < \alpha$) [3]. To better understand the self-acceleration process, it is essential to obtain accurate values of acceleration exponent α and fractal excess d of the flame.

The empirical constant A is essential for the self-accelerating flame regime, and its value remains relatively independent of the experimental

* Corresponding author.
E-mail address: J.Yang@leeds.ac.uk (J. Yang).

https://doi.org/10.1016/j.fuel.2023.129182
Received 14 April 2023; Received in revised form 6 June 2023; Accepted 5 July 2023
Available online 10 July 2023

Nomenclature

A	Constant in power law equation
A_f	total surface area (mm^2)
A_X, A_G,A_B	empirical constants calculated by different theoretical expressions ($m/s^{1.25}$)
B	flame speed pulsation amplitude (m/s)
c_p	specific heat at constant pressure (J/kg·K)
d	fractal excess
E_a	activation energy (J)
f	frequency (s^{-1})
k	thermal conductivity (J/m/K/s)
K	empirical constant
L_b	flame speed Markstein length (m)
Le	Lewis number
Le_E	Lewis number of excessive reactants
Le_D	Lewis number of deficient reactants
Le_{eff}	effective Lewis number, Eq. (8)
Ma	Markstein number
Ma_b	burned gas Markstein number
n	wavenumber (mm^{-1})
n_{max}	maximum wavenumber (mm^{-1})
n_{min}	minimum wavenumber (mm^{-1})
$n^*_{\min}$	minimum wavenumber when $r \to \infty$(mm^{-1})
Pe	Peclet number r_u/δ
Pe_{cl}	critical Peclet number r_{cl}/δ
P_i	initial pressure (MPa)
Pr	Prandtl number
r	flame radius (mm)
r_{cl}	critical flame radius (mm)
r_u	cold flame front radius (mm)
R^o	gas constant (J/(K·mol))
S_n	propagation flame speed (m/s)
S_s	unstretched propagation flame speed (m/s)
t	time after spark ignition (s)
T_{ad}	adiabatic flame temperature (K)
T_i	initial temperature (K)
T_u	temperature of the fresh mixture (K)
u_l	unstretched laminar burning velocity (m/s)
Ze	Zel'dovich number

Greek symbols

α	acceleration exponent
δ	flame thickness (mm)
δ_k	preheat zone flame thickness (mm) $(k/C_p)_{T^o}/(\rho_u u_l)$
κ	thermal diffusivity (m^2/s)
λ	phase difference
ν	kinematic viscosity (m^2/s)
ρ	density (kg/m^3)
ρ_b	burned gas density (kg/m^3)
ρ_u	unburned gas density (kg/m^3)
σ	ratio of unburned gas density to burned gas density ρ_u/ρ_b
σ_{sd}	standard deviation
ϕ	equivalence ratio
Φ	mass of excess to deficient reactants in the fresh mixture relative to their stoichiometric ratio
Λ	wavelength (mm)
Λ_{min}	minimum wavelength (mm)
Λ_{max}	maximum wavelength (mm)
Γ	constant Pe/n_{max} (mm)

initial conditions. Gostintsev et al. [3] investigated the self-accelerating flame propagation of various air–fuel mixtures, and corroborated the dependence of the propagation law on the physicochemical parameters of the mixture, mainly the laminar burning velocity (u_l) and the thermal diffusivity of the mixture (κ). These dependencies arise from the assumption that the elements of the laminar flame play a role in the self-accelerating or self-turbulent zone of combustion:

$$A = a(\sigma)u_l^2/\kappa^{0.5} \tag{3}$$

where κ is the thermal diffusivity, u_l is the unstretched laminar burning velocity,σ is the volumetric expansion ratio expressed as the ratio of the density of unburnt to burnt gases, ρ_u/ρ_b. $a(\sigma)$ is a dimensionless function of σ, can be expressed as $0.002\sigma^2$ when assuming $\alpha = 1.5$ and $\kappa = 1.5 \times 10^{-5}$ m^2/s for all the mixtures. This yields an empirical expression of A:

$$A_G = \frac{0.002\sigma^2 u_l^2}{\kappa^{1/2}} \tag{4}$$

Later, Bradley et al. [4] made a mathematical deduction based on fractal theory and proposed a modified expression of A:

$$A_B = \frac{0.554\sigma^{3/2}u_l^2 K^{1/2}}{\nu^{1/2}Pe_{cl}^{1/2}} \tag{5}$$

where K is the empirical constant, which can be estimated from [4].

Note that the above two empirical expressions are both derived based on the assumption that $\alpha = 1.5$, which is not always valid for practical flame propagations. Values of α reported in the literature are summarized in Table 1. However, these empirical expressions, Eqs. (4) and (5), were misused to determine the transient acceleration exponent using the ad hoc assumption $\alpha = 1.5$ [10–14]. For example, Kim et al. [10] analyzed the large-scale explosion of methane and hydrogen gases, and observed that α extracted from A_G is<1 (corresponds to $d < 0$) after the instability. This indicates that the flame speed does not increase, which is contrary to the common sense of flame speed acceleration. Other authors replicated the misuse of Eqs. (4) and (5) in [11–14]. Given the large discrepancy between the actual and the assumed values of the acceleration exponent, the expression of A needs to be carefully reexamined. Furthermore, it is important to acknowledge that the acceleration exponent α is a model parameter rather than a physical parameter [12]. As indicated in Table 1, there is a substantial variation or dispersion in the values of α. The determination of α is significantly influenced by the choice of extraction method and the range of flame radii used for processing. In order to gain a comprehensive understanding of the extraction methods and to investigate the universality of self-acceleration, a summary of previous extraction methods for acceleration exponents is provided in Table 2.

Moreover, it is reported that the acceleration exponents vary with the mixture condition [1]. As summarized in Table 1, various values of the acceleration exponent have been reported experimentally via different power-law correlations. Gostintsev et al. [3] evaluated the large-scale explosive experiments with various mixtures at atmospheric pressure undertaken by Lind and Whitson [15], and concluded that all mixtures exhibited an identical accelerate exponent value of 1.5. More notably, the initial stated value of α was reduced to 1.25–1.5 in the subsequent studies [16,17], and the updated evaluation indicated that the value of 1.5 was only obtained in a few situations. Kwon et al. [18] investigated $H_2/O_2/N_2$ flames in a constant high-pressure dual-chamber vessel at a pressure of up to 1.5 MPa. The acceleration exponent varies from 1.23 to 1.36 for different equivalence ratios. Haq [19] conducted tests in a combustion chamber with an ambient methane/air flame. The results suggest that α is 1.24 in the horizontal direction and 1.32 in the vertical direction. To describe the development of cellular-flame instabilities, Bauwens et al. [9] conducted large-scale experiments at atmospheric pressure using propane–air mixtures, and found that the

Table 1
Previous experimental studies of acceleration exponents, including the present study.

Authors	Year	α	Fuel	Experimental setup
Gostintsev et al. [3]	1988	1.5	$H_2/C_2H_2/C_3H_8/CH_4/C_2H_4O/C_4H_6/O_2$	Large scale
Gostintsev et al. [16]	1999	1.25–1.5	/	Large scale
Gostintsev et al. [17]	2004	1.25–1.5	/	Large scale
Bradley et al. [4]	1999	1.5	CH_4,C_3H_8,H_2	Large scale
Bradley et al. [6]	2000	1.5	CH_4,C_3H_8	Large scale
Kwon et al. [18]	2002	1.23–1.36	$H_2/O_2/N_2$	Small scale
Haq et al. [19]	2005	1.24, 1.32	CH_4	Small scale
Wu et al. [1]	2013	1.2–1.36	H_2	Small scale
Bauwens et al. [9]	2015	1.2–1.4	C_3H_8	Large scale
Yang et al. [22]	2016	1.2–1.4	H_2	Small scale
Okafor et al. [23]	2016	1–1.36	H_2/CH_4/air mixtures	Small-scale
Bauwens et al. [24]	2017	1.32 ± 0.01	H_2 (ϕ = 0.33–0.57)	Large scale
Kim et al. [20]	2018	1.1–1.4	H_2	Small scale
Huo et al. [2]	2018	1.2–1.4	H_2	Small scale
Huang et al. [25]	2019	1.13–1.17	H_2	Small scale
Kim et al. [21]	2020	1.25–1.43	H_2	Small scale
Cai et al. [12]	2020	1–1.27	$H_2/O_2/N_2$	Small scale
Zhao et al. [26]	2023	1–1.25	$H_2/O_2/N_2$	Small scale
Present study	2023	1.125–1.39	H_2	Small scale

value of α varies between 1.2 and 1.4. Kim et al. [20,21] investigated hydrogen cellularity in a high-pressure combustion chamber, and found that the values of α and d sit in the range of 1.1–1.4 and 0.1–0.3, respectively. Yang et al. [22] investigate spherically expanding $H_2/O_2/N_2$ flames at various pressures, equivalence ratios, and thermal expansion ratios. The acceleration exponent is estimated to be between 1.2 and 1.4. Okafor et al. [23] studied cellular instability in spherical propagating hydrogen-methane-air flames in a constant volume chamber and found that for hydrogen fraction <50%, the exponent α fluctuates from 1 to 1.26, which is in good agreement with Kwon et al. [18] and Wu et al. [1]. Huo et al. [2] also found that the value of the hydrogen acceleration exponent is about 1.2–1.4. The experiments and quantitative evaluation were conducted on the cellular morphology and self-acceleration in lean H_2-air expanding flames by Huang et al. [25] with values of α between 1.13 and 1.17 at elevated pressure. Cai et al. [12] introduced two distinct acceleration exponents: the transition acceleration exponent and the self-similar acceleration exponent. Furthermore, they proposed an empirical power-law correlation for α, which aims to encompass the entire self-acceleration process. Evidently, the majority of α values fall within the range of 1.1 to 1.4, rather than the expected value of 1.5. This lack of consensus regarding the precise value of α undermines the validity of the empirical expression for the constant A, which was originally derived based on the assumption of $\alpha = 1.5$.

Moreover, the local cascading mechanism in the cell structure may cause the surface area to grow faster and slower alternately instead of a continuous increase, which leads to a non-linear climbing sinusoidal waveform in the history of flame speed [27,28]. The actual self-acceleration process exhibits strong and weak acceleration phases. The classical power-law expression could not capture such a so-called global pulsation pattern. Therefore, it is necessary to take into account this unique pulsation when analyzing flame self-acceleration.

It should also be highlighted that this global pulsing phenomenon is implicitly embedded in previous modelling work [29], albeit its significance and mechanism have not been appreciated until subsequent DNS [30] and experimental [2,27] studies. However, there is a dearth of associated experimental data, particularly in terms of quantitative data. In addition, thermo-acoustic instability also induces speed fluctuation during flame expansion [31]. However, the role of thermo-acoustic instability in self-acceleration remains unclear and this effect has been omitted in previous studies on global pulsing acceleration patterns [2,27]. Indeed, the effects of global pulsing acceleration and thermo-acoustic instability on flame speed oscillations should be investigated and discriminated.

Since self-acceleration occurs not only in laminar combustion regimes, but also in many turbulent combustion applications [32], the determination of the acceleration exponent is useful for accurate predictions of the propagation of premixed flames. Though plenty of experimental and numerical work has been conducted to address the self-acceleration of the hydrogen-air mixture, it is worth recalling that, firstly, the existing turbulent combustion models do not account for laminar flame instabilities manifest in the development of cellular patterns on the surface of a laminar flame. Additionally, lean hydrogen-air flames are always unstable. Therefore, it is necessary to revisit hydrogen flames and reassure its acceleration factor in a timely manner given the potential of hydrogen to replace hydrocarbons derived from natural gas and crude oil.

In light of the above considerations, the present study aims: (i) to develop and validate a suitable method to incorporate the pulsation pattern into the self-acceleration process; (ii) to investigate the acceleration exponents for hydrogen-air flames over a wide range of initial conditions and hence propose a modified general expression of constant A, which is useful for evaluating deflagration and explosion waves; (iii) to explore and characterize the intrinsic parameters of global pulsation of hydrogen-air flames, which is essential for understanding the dependence of the intensity of the DL and thermal diffusion instability in this significant issue; (iv) to get a better understanding of its fundamental significance in generating pulsatile flame speed through the nonlinear generation rate of cells.

Table 2
Extraction methods of acceleration exponents.

No.	Fitting expression	Disadvantages
1. [3,4,6]	$r = r_{cl} + At^{\alpha}$	Diverse ignition conditions can introduce a time shift, leading to a notable bias in the extraction of α.
2. [12]	$\frac{dr}{dt} = \alpha A^{1/\alpha}(r - r_{cl})^{(\alpha-1)/\alpha}$	This expression is not valid for capturing the onset of self-acceleration, as it implies a zero-flame propagation speed.
3. [1]	$\frac{dr}{dt} = \alpha A^{1/\alpha} r^{(\alpha-1)/\alpha}$	This equation would overestimate the α in measurements because the rcr term is dropped.
4. [9]	$\frac{dr}{dt} / \left(\frac{dr}{dt}\right)_{cl} = (r/r_{cl})^{(\alpha-1)/\alpha}$	This equation is valid under the assumption that $r \gg r_{cl}$.
5. [12]	$r = r_{cl} + A(t - t_{cl})^{\alpha}$	This equation fails to account for the oscillation growth of the flame propagation.

Where r_{cl} is critical flame radius corresponding to the onset of self-acceleration, t_{cl} is critical time corresponding to the onset of self-acceleration after ignition.

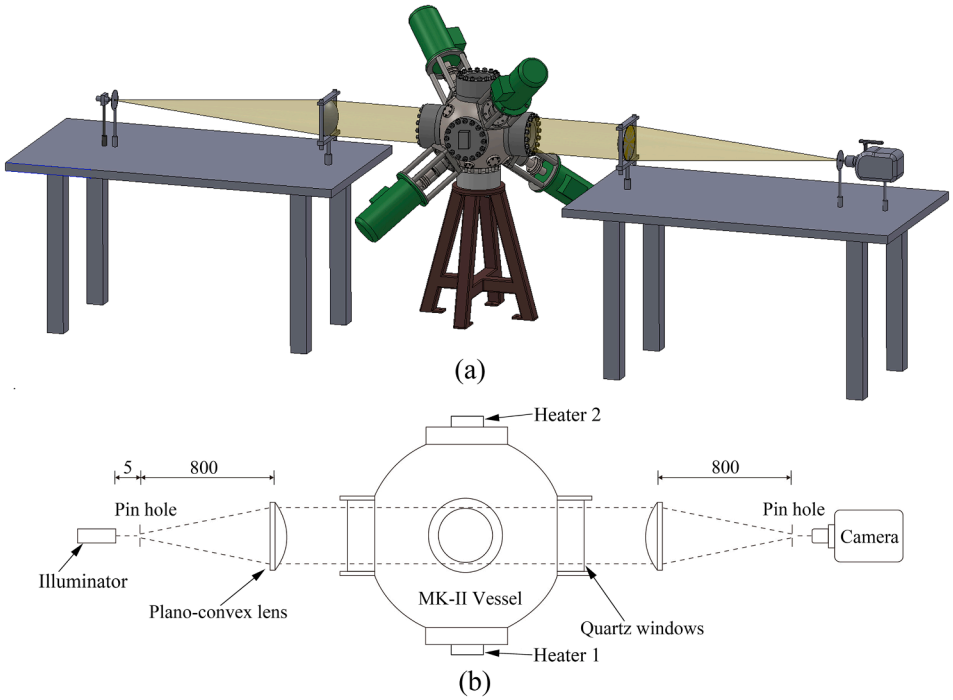

Fig. 1. MK-II vessel with Schlieren imaging apparatus employed in this research. (a) 3D diagram of Schlieren imaging system; (b) Schematic diagram of the optical setup (top view). The unit is mm.

2. Cell size calculations

A smooth, stable, propagating flame becomes unstable spontaneously, resulting in a structure comprised of different size cells in dynamic equilibrium. The smaller cells are in a constant state of destabilisation and re-stabilization. The cell becomes unstable as it grows in size because the localised stretch rate on the cell surface drops. Fissioning into smaller cells with higher localised stretch rates allows it to re-stabilize [6]. Since cascading of the cells occurs continuously, the stages with faster and slower acceleration repeat themselves. Throughout the cycle of strong and weak acceleration phases, the unstable flame shows a global pulsing acceleration pattern with a certain frequency. Therefore, it is interesting to know the relationship between cell size and the frequency, amplitude of global pulsation. The theory for calculating mean cell size, proposed in [33] is discussed below.

The unstable flame is accompanied by a cellular spectrum in a range of perturbing wavelengths with upper and lower limits, or cutoffs ($\Lambda_{min} < \Lambda < \Lambda_{max}$) according to the linear stability theory [12]. The disturbances caused by wavelengths larger than the maximum wavelength (Λ_{max}) are stabilised by the flame stretch. Short-wavelength less than the minimum wavelength (Λ_{min}) disturbances are stabilized by diffusion effects. According to the stability analysis in [33], the wavelength corresponding to the smallest cell size approached a constant value as the flame expands, and cells with smaller sizes disappeared. These stabilization mechanisms are validated by experiments [6,25], hence it is appropriate to adopt Λ_{min} as the mean cell size for the fully-developed cellular flames.

The minimum wavelength can be calculated as: $\Lambda_{min} = 2\pi r/n_{max}$. Here, n, is essentially a wavenumber, theoretically the ratio of the circumference of the flame to the wavelength (i.e., the cell size or diameter) at the corresponding moment. Furthermore, Peclet number, Pe ($= r_u/\delta$) is linearly related to n_{max}. Setting $Pe/n_{max} = \Gamma$, it follows that:

$$\Lambda_{min} = 2\pi r/n_{max} = 2\pi\delta\Gamma \tag{6}$$

Here δ is the flame thickness. Given thermal diffusion is the stabilising mechanism in this case, Γ obviously depends on Le_{eff} and Pr as well [33]:

$$\Gamma = \left[C_1 + Ze\left(Le_{eff} - 1\right)C_2 + PrC_3\right]/C_4 \tag{7}$$

where C_1, C_2, C_3, C_4 are the modified factors, more details are given in Ref [33], Ze is Zel'dovich number, $= E_a(T_{ad} - T_u)/\left(R_0 T_{ad}{}^2\right)$, in which T_{ad} the adiabatic flame temperature, T_u the temperature of the fresh mixture, E_a the activation energy ($-2R_0[\partial\ln(\rho_u u_l)/\partial(1/T_{ad})]$), and R^o the universal gas constant. Pr is Prandtl number ($\nu/\kappa = (\mu/\rho)/[k/(c_p\rho)] = c_p\mu/k$), μ is the dynamic viscosity (kg/m/s), k is the thermal conductivity, (J/m/K/s), c_p is specific heat,(J/kg/K), ρ is the density (kg/m^3).

The Lewis number is defined as the ratio of thermal to mass diffusivity of deficient reactants. The accuracy of assessments based on a single Lewis number, however, is expected to be reduced in comparison to tests performed under a variety of circumstances [33]. Therefore, according to Fick's law for binary mixtures, the effective Lewis number is proposed based on the binary mass diffusivity in a reactant-inert mixture. In a global reaction scheme where fuel and oxidizer interact to form products, the mixture is identified by two separate Lewis numbers, Le_E and Le_D, which stand for the reactant that is comparatively in excess or deficient, respectively. Following that, the examination of the flame zone reveals that these two merge to form a single efficient Lewis number [33]:

$$Le_{eff} = 1 + \frac{(Le_E - 1) + (Le_D - 1)\mathscr{A}}{1 + \mathscr{A}} \tag{8}$$

where $\mathscr{A} = 1 + Ze(\Phi - 1)$ is a measure of the strength of the mixture. Φ is defined as the ratio of the mass of excess to deficient reactants in the fresh mixture relative to their stoichiometric ratio. In other word, $\Phi = \phi$ for fuel rich mixtures, and $\Phi = 1/\phi$ for fuel lean mixtures.

The definition of flame thickness provided can only be applied to flames characterized by a chemically inert preheat zone. However, the applicability of the traditional equation for hydrogen flames becomes questionable in this context because the assumption of a chemically inert preheat zone is invalid. In hydrogen flames, H atoms exhibit rapid diffusion towards the leading edge, where they initiate reactions to a greater extent compared to hydrocarbon flames. Consequently, the

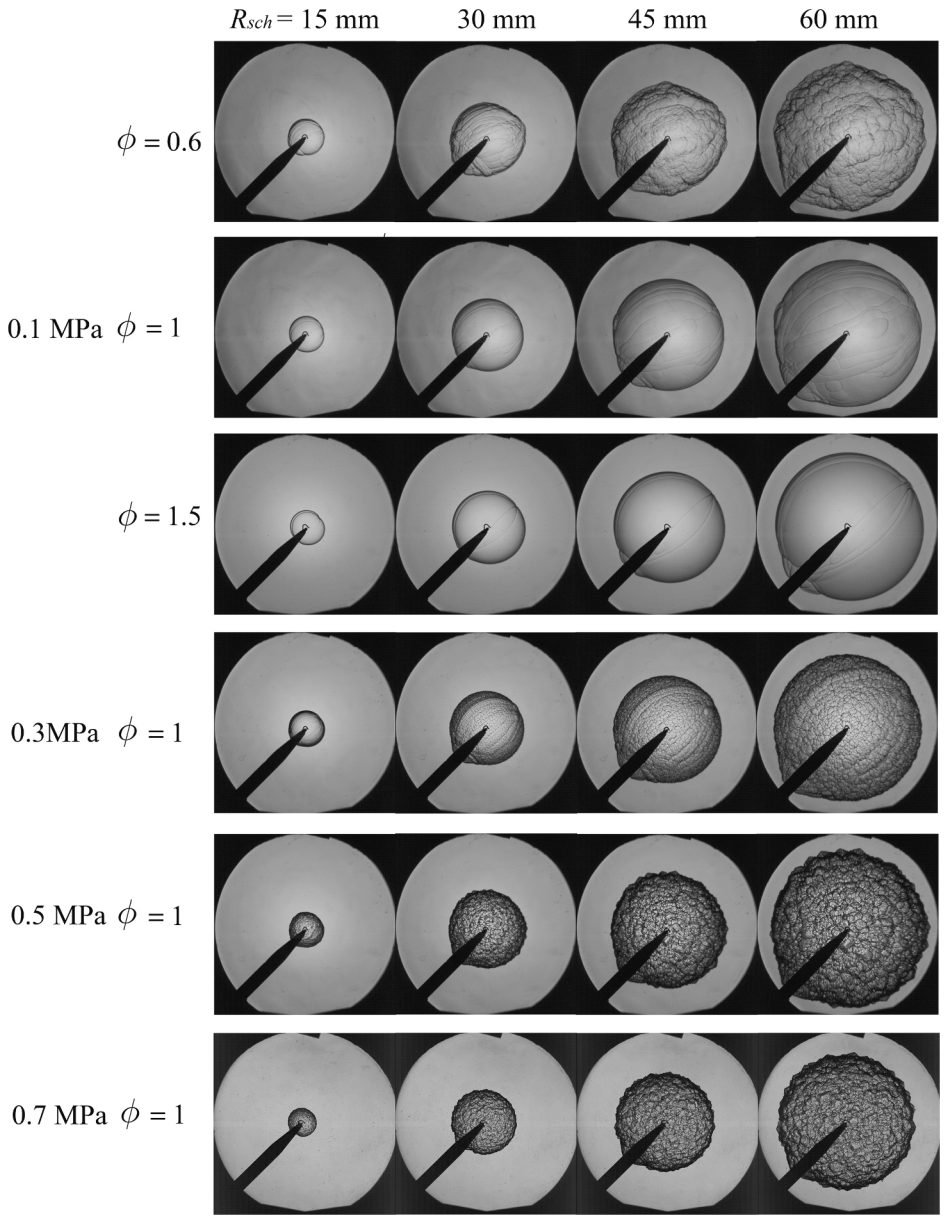

Fig. 2. Flame front morphology and evolution of hydrogen-air mixtures under different equivalence ratios (0.6, 1.0 and 1.5) and initial pressures (0.1, 0.3 and 0.5 MPa) with a fixed initial temperature of 360 K.

preheat zone in hydrogen flames is significantly reduced. As a result, the calculation of flame thickness using the specified method, known as the preheat zone flame thickness δ_k, is obtained through the following expression [34]:

$$\delta_k = \frac{(k/c_p)_{T^0}}{\rho_u u_l} \tag{9}$$

where $(k/c_p)_{T^0}$ is the ratio of thermal conductivity and specific heat at a certain inner layer temperature, T^0. The values of T^0 for different gases are presented in [34]. The other parameters are obtained from GASEQ code [35].

3. Apparatus

The experiments were conducted in a spherical stainless steel combustion vessel (MK-II), with an inner chamber diameter of 380 mm and a maximum observable flame diameter of 150 mm, as shown in Fig. 1. The vessel and mixture were heated, using two internal 2 kW coiled heating elements, and gas temperature can be measured with a sheathed chromel–alumel thermocouple. Four fans, driven by 8 kW three-phase motors, were mounted on the inner wall of the combustion vessel, to mix the reactants. The combustible premixed mixture inside the combustion vessel was centrally ignited by a spark plug. The morphology and propagation of the flame were captured by high-speed Schlieren cinéphotography using pinhole (light source provided by a MI-150 Fiber Optic Illuminator) recorded with a digital camera (Ultra High-Speed Phantom v2512, AMETEK) at 30,000 frames per second (fps) and 0.263 mm/pixel resolution. The minimum flame radius was selected as 6 mm, to eliminate the effect of the initiating spark plasma. A central spark plug was employed with minimal ignition energy of roughly 1 mJ to eliminate any substantial disturbances during flame propagation. More details of this apparatus and the experimental procedure are provided in [36–38]. The measured instantaneous Schlieren cinéphotography flame radius, defined as $R_{sch} = \sqrt{A_f/\pi}$, where A_f is the area of the 2D-projection of the flame.The derivations of some parameters including cold flame front radius, r_u, stretched flame speed, S_n, burned

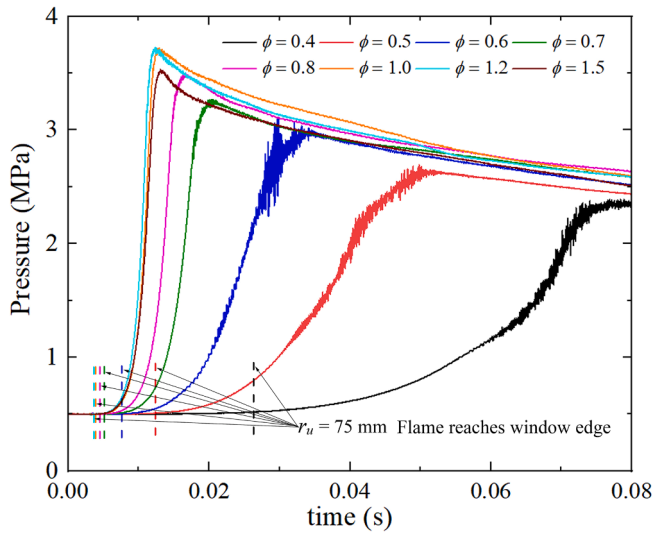

Fig. 3. Pressure records from spherically expanding laminar hydrogen-air flames at the initial conditions of 0.5 MPa and 300 K.

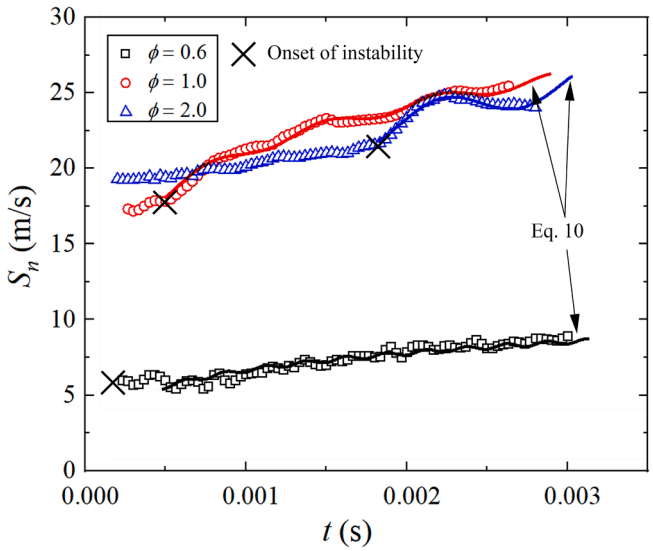

Fig. 4. Propagation flame speeds S_n against t for hydrogen-air flames at 300 K and 0.3 MPa. The solid curves are fitting lines using Eq. (10).

gas Markstein length, L_b, unstretched laminar burning velocity, u_l, burned gas Markstein number, Ma_b, critical Peclet number, Pe_{cl} are discussed in [36] and supplementary. The experiments were conducted over a wide range of initial pressures (P_i = 0.1, 0.3, 0.5, 0.7 MPa), temperatures (T_i = 300, 360, 400 K) and equivalence ratios (ϕ = 0.4, 0.6, 0.8, 1, 1.2, 1.5, 2.0). The experimental repeatability was checked through three explosions at each experimental condition. The standard deviation method (σ_{sd}) is used for calculating uncertainties represented by error bars.

4. Results and discussions

4.1. Flame morphology

A set of typical image sequences of experimentally observed hydrogen-air flames at different conditions is shown in Fig. 2. At 0.1 MPa, large cracks appear over the flame surface at the stoichiometric (ϕ = 1) condition. Forϕ = 0.6, $Le_{eff} < 1$, the flame surface is highly wrinkled, especially at large radii, r_u = 60 mm. For ϕ = 1.5, $Le_{eff} > 1$, only a few cracks appear on the flame surface. When $Le_{eff} < 1$, the flame curvature focuses diffusion of enthalpy into the flame. Then the conductive heat fluxes are lost out of the crest of the flame front, and the local burning velocity rises, but a contrary effect occurs in the flame surface trough, where diverging gas flow decreases the burning velocity and local temperature. As a result, the flame deforms more and becomes more unstable. For $Le_{eff} > 1$, the DL instability is neutralised by thermal diffusion processes, which result in a lower burning velocity at the top of the flame front, thereby stabilising the flame. For stoichiometric hydrogen-air flames, the cellular structure appears earlier at higher pressure, and higher pressure results in the flame surface folding more sharply, demonstrating the manifestation of DL instability for the reduced flame thickness due to the increased pressure. With an increase of initial unburned temperature, the destabilizing propensity of the hydrogen-air flames is slightly reduced, in agreement with [36].

4.2. Global pulsation of unstable flames

Previous studies considered the propagation speed of self-accelerating flames as a monotonous increase process, which leads to a linear correlation of flame speed, Eq. (2). However, recent experiments observed a pulsatory pattern of flame speed [2,27]. Given its fundamental and practical significance, further characterization and understanding of the mechanism of this pulsatory pattern are necessary.

4.2.1. Effects of thermo-acoustic instability

Thermo-acoustic instability occurs when the heat release rate fluctuations are in phase with the acoustic pressure oscillations inside the combustor [39]. The thermo-acoustic instability in the current vessel has been studied in previous work [31]. It is concluded that, fuels with low burning rates, like *iso*-octane, were more likely to be affected by acoustic instabilities due to the high rate of change of heat release rate as a consequence of the acoustic wave. For fuels with high burning rates, like hydrogen, the acoustic instabilities were weaker, and less pronounced in the rich mixtures. Such weak acoustic instability has a negligible effect on both the power-law form and the index of acceleration, as well as on the strong pulsation of flame speed. This was revised here. The temporal variation of the pressure signal was recorded for centrally ignited spherical laminar hydrogen-air explosions, as shown in Fig. 3. The pressure in the combustion chamber remains constant and oscillate-free before the flame reaches the observable edge of the optical window. Pressure oscillations due to thermo-acoustic instability happen only in relatively lean conditions at the end of combustion when the acoustic wave starts to interact with the flame. However, the pulsatory fluctuation of flame speed in this study occurred within the window edge of the combustion chamber (75 mm); therefore, the effects of thermo-acoustic instability can be excluded in the current study.

4.2.2. Pulsation formula of flame speed

The temporal evolution of the flame speed for hydrogen-air mixtures at ϕ = 0.6, 1.0, 2.0, T_i = 300 K and P_i = 0.3 MPa is presented in Fig. 4. The specifics of how to identify the onset of instability (marked by × symbol in Fig. 4) are discussed in [36]. The pulsating feature of flame speed becomes obvious once the onset of instability occurs, especially under fuel-rich conditions. In other words, the richer the mixture, the higher the magnitude of oscillation, and the lower the frequency. The variation of the equivalence ratio from 0.6 to 2.0 corresponds to Le_{eff} rising from 0.63 to 1.41 calculated by Eq. (8). As shown in Section 3.1 and Fig. 2, for Le_{eff} value less than unity, the flame features a strongly wrinkled surface and a high frequency and small amplitude in oscillating flame speed. When Le_{eff} is greater than unity, the results are the opposite. For $Le_{eff} \geq 1$, the power-law correlation of flame speed in Eq.2 is inadequate to capture the self-acceleration pattern with evident oscillations. Therefore, a new term of sinusoidal function was added to the power-law correlation to take account of the pulsatory behavior:

$$S = A\alpha t^{\alpha-1} + B\sin(2\pi ft + \lambda) \quad (10)$$

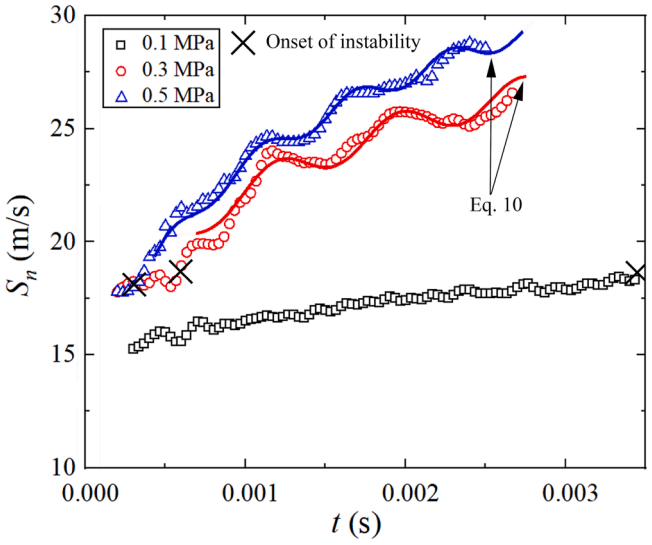

Fig. 5. Propagation flame speeds S_n against time for hydrogen-air flames at 300 K and $\phi = 1.2$. The solid curves are fitting lines using Eq. (10).

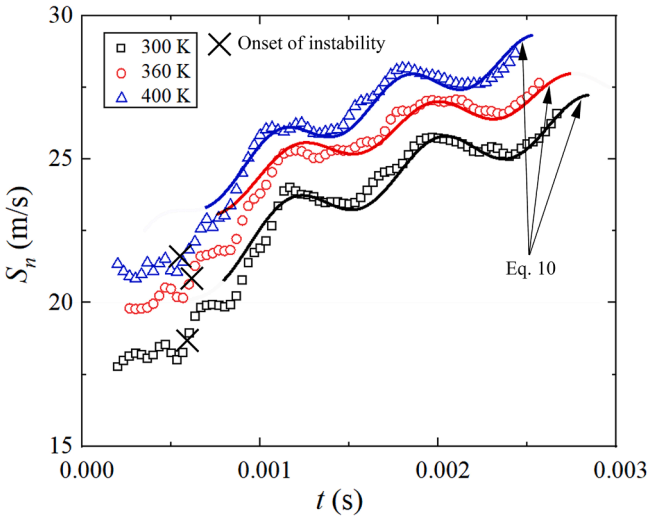

Fig. 6. Propagation flame speeds S_n against t for hydrogen-air flames at 0.3 MPa and $\phi = 1.2$. The solid curves are fitting lines using Eq. (10).

where f is frequency, B is amplitude and λ is phase difference. To obtain constant A, acceleration exponent α, frequency f, amplitude B and phase difference λ for each condition, a least-square fitting method is used to fit the data using Eq. (10). The relationship between waveform and X-axis position (time) is determined by the phase difference, λ, which is not explored in depth in this study for no specific physical significance. All derived parameters are summarized in Appendix A1. The assessment of each parameter has been discussed in the following sections.

The underlying mechanism of pulsatory flame speed is relevant to the fission process of cellular structuring on the flame surface. The cells over the flame surface grow larger as the flame expands, increasing the flame surface area and speed. A cell splits into two or more cells when its size surpasses the cut-off threshold. During the splitting process, both the rising rate of surface area and the total combustion rate of the flame decrease, lowering overall acceleration. The freshly produced smaller cells begin to develop when the division process ends, the overall growth rate increases, and the flame accelerates. The slower phases of acceleration will continue to reoccur while the cell cascade proceeds. As shown in Figs. 5 and 6, the predicted flame speeds (solid curves) via the comprehensive expression (Eq. (10) match the measurement under different pressures and temperatures. Additionally, each fitting has a high goodness-of-fit score ($R^2 > 0.95$). As shown in Fig. 5, the higher the pressure, the faster the flame cell development and subsequent division, resulting in a higher frequency and smaller fluctuation range of flame speed oscillation. The reason is that the high pressure enhances the intensity of hydrodynamic instability causing intense folds over the flame surface (see Fig. 2). Additionally, increasing temperature from 300 K to 400 K enhanced the pulsation frequency mildly, but the variation in amplitude is negligible as shown in Fig 6.

4.3. Acceleration exponent and fractal excess

The acceleration exponents, α, extracted from experimental data using Eq. (10) are plotted against ϕ for hydrogen-air mixtures under various conditions, as shown in Fig. 7. The acceleration exponents from the present work are consistent with previous studies [1,20,24] (Fig. 7a). Firstly, the values of α for lean mixtures are higher than those of rich mixtures in the most cases, which means the flame speed of lean mixture ($Le_{eff} < 1$, negative or low Markstein number) accelerates faster than rich mixtures ($Le_{eff} > 1$, positive or high Markstein number). Thermal diffusion instability causes strong wrinkles for lean mixtures and weak wrinkles for rich mixtures by destabilizing or stabilizing (suppressed by hydrodynamic instability) these mixtures, respectively. Alternatively, the acceleration exponents, α, also capture the capacity for flame acceleration. Previous research has revealed that mixtures with Lewis numbers below unity and negative Markstein numbers tend to exhibit acceleration at the leading edge [40–43]. These findings

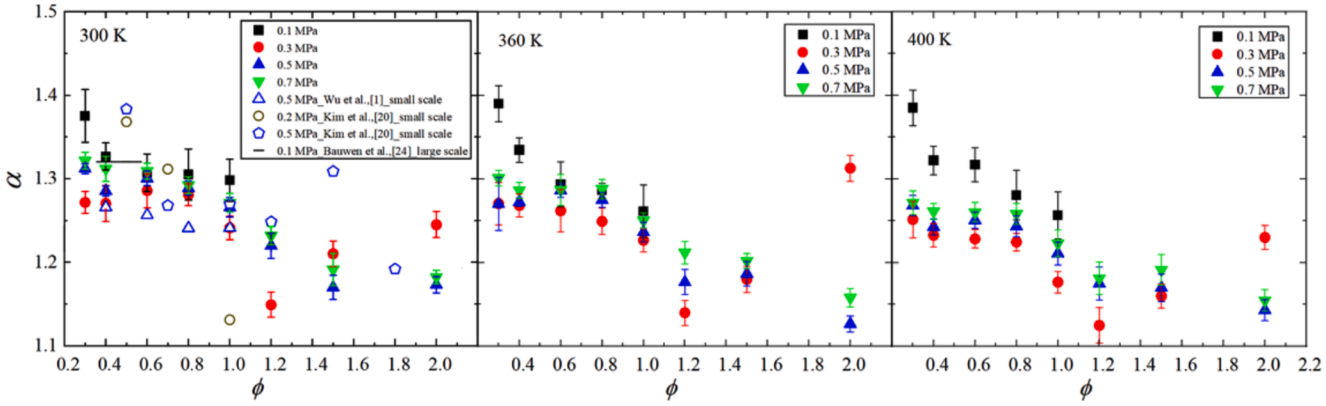

Fig. 7. Experimentally extracted acceleration exponents, α, for hydrogen-air combustion at various conditions using Eq. (10).

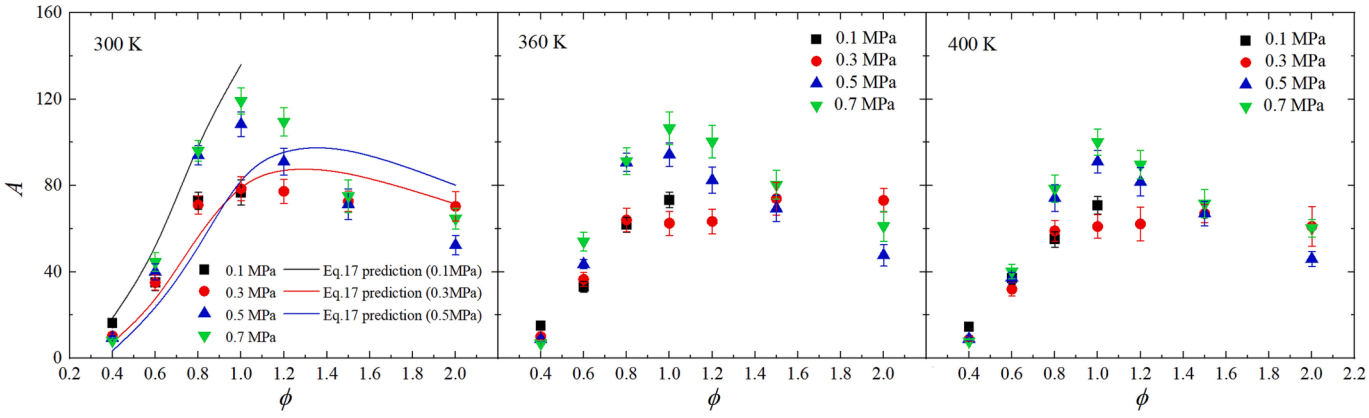

Fig. 8. The experimental and calculated constants A against ϕ at different initial temperatures.

highlight the significance of considering the interplay between Lewis numbers, Markstein numbers, and flame acceleration in understanding and predicting flame behavior. Additionally, the variations in initial pressures (ranging from 0.1 to 0.7 MPa) and temperatures (ranging from 300 to 400 K) within considered conditions do not seem to have notable individual impacts on the accel the acceleration exponents. Furthermore, the experimental study conducted by [24] on lean hydrogen-air mixtures with equivalence ratios ranging from 0.33 to 0.57, carried out in a 64 m^3 constant-pressure enclosure, employed detailed front tracking techniques to measure flame diameters up to 1.2 m. These large-scale experimental results were utilized to validate the small-scale experimental findings presented in this study, and a high level of agreement between the two sets of results was observed. This validation provides compelling evidence to support the conclusion that the size effect does not significantly impact the acceleration exponents, and signifies that small-scale laboratory explosions can serve as indicators or predictors of the flame speeds observed in larger atmospheric conditions.

The fractal excess d is determined via Eq. (2) with the data of the acceleration exponent, α from Fig. 7. Note that the value of α for hydrogen-air mixtures in the present study ranged from 1.125 to 1.39, almost around value of 1.25. Indeed, α reported in the literature (Table 1) fluctuates around a similar range over various fuels and conditions. Moreover, two-dimensional simulations of radially expanding flames in cylindrical geometry display a radial growth with 1.25 power-law temporal behavior after some transient time [44]. The α value of 1.5 and d value of 1/3 would likewise not be appropriate for the hydrogen-air mixture.

4.4. Theoretical constant a

It is of paramount importance to obtain a reasonable theoretical expression for constant A to better quantify the self-accelerating state of an outwardly propagating flame. If a flame radius is large enough for flame-stretch rates to be small, the ratio of the flame speed referred to the mean radius arising from the surface wrinkling, S_n, to the unstretched laminar flame speed, S_S, equals the ratio of the wrinkled to the smooth surface area [33]:

$$S_n/S_s = (n_{max}/n_{min})^d \tag{11}$$

Due to the mass conservation states $S_s = u_l\sigma$, gives:

$$S_n = \sigma u_l (n_{max}/n_{min})^d \tag{12}$$

where n_{min} rapidly approaches the constant $n^*_{\min}$ after the instability. In addition, it can be supposed that the spectrum of unstable wavelengths during the fractal-like wrinkling is close to what the linear stability theory predicts, thus [33]:

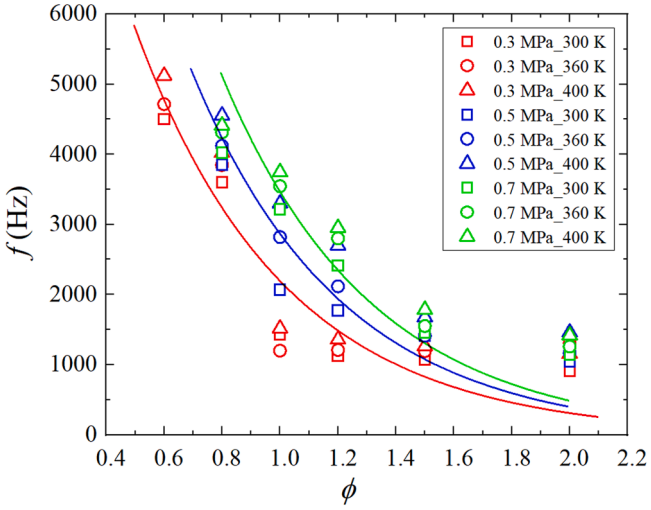

Fig. 9. Pulsation frequencies f for global pulsation in hydrogen-air flames at P_i = 0.3, 0.5 MPa. The curves are fitting lines using Eq. (18).

$$n_{max} \sim (r - r_{cl})/\delta\Gamma \tag{13}$$

where Γ is given by Eq.7. Following the integration of Eq. (12), the propagation speed is discovered to be:

$$S_n = \left(\frac{(1-d)\sigma^{\frac{1}{d}}\Gamma n^*_{min}}{\kappa Pe_{cl}}\right)^{\frac{d}{1-d}} u_l^{\frac{d+1}{1-d}} t^{\frac{d}{1-d}} \tag{14}$$

Due to $S_n = A \bullet \alpha \bullet t^{\alpha-1}$, therefore:

$$A_X = \left(\frac{(1-d)\sigma^{\frac{1}{d}}\Gamma n^*_{min}}{\kappa Pe_{cl}}\right)^{\frac{d}{1-d}} u_l^{\frac{d+1}{1-d}} (1-d) \tag{15}$$

The newly accepted α value of 1.25 was used as the established foundation in Eq. (15) for the general utilization of hydrogen/air flames:

$$A_X = 0.757\left(\frac{\sigma^5\Gamma n^*_{min}}{\kappa Pe_{cl}}\right)^{1/4} u_l^{3/2} \tag{16}$$

where n^*_{min} is a function of σ alone ($n^*_{min} \approx 7$ for a typical value of $\sigma = 6$), independent of the Prandtl number, the Lewis number, and the equivalence ratio[33], then get a generic form:

$$A_X = 1.231\left(\frac{\sigma^5\Gamma}{\kappa Pe_{cl}}\right)^{1/4} u_l^{3/2} \tag{17}$$

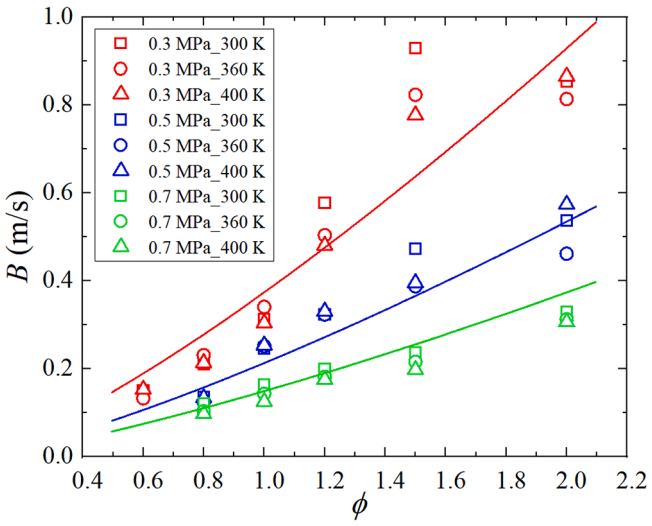

Fig. 10. Pulsation amplitudes B for global pulsation in hydrogen-air flames at P_i = 0.3, 0.5 MPa. The curves are fitting lines using Eq. (19).

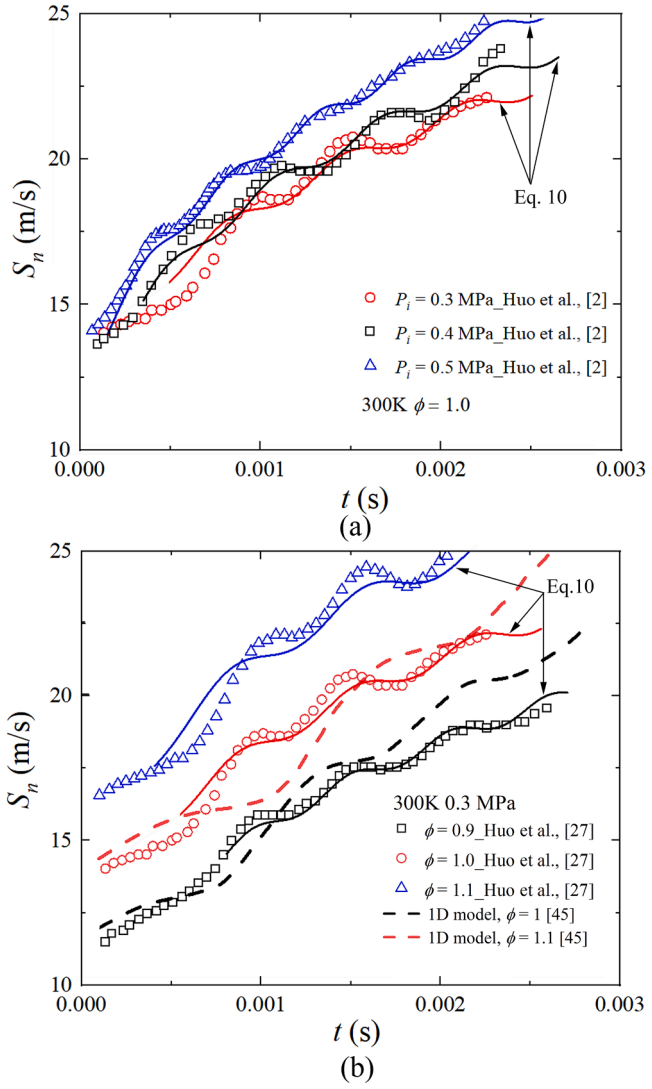

Fig. 11. Propagating flame speeds S_n against t for hydrogen-air flames (a) Ref. [2] at 300 K and ϕ = 1.0. (b) Ref. [27] and 1-D model [45] at 300 K and 0.3 MPa.

The constant A extracted from experimental data using Eq. (10) are plotted against ϕ for hydrogen-air mixtures under various conditions, as shown in Fig. 8. It appears that the constant A decreases when the conditions are far from stoichiometric and increases when they are near to stoichiometric. Utilizing the parameters, u_l, Pe_{cl}, etc., obtained from reference [36], the value of A_X that has been derived from Eq. (17) demonstrate a satisfactory level of agreement with the experimentally derived A.

4.5. Frequency and amplitude of pulsatory flame speed

A comprehensive frequency database of hydrogen-air combustion is presented in Fig. 9. The frequency decreases exponentially from 0.6 to 2.0. Since Le_{eff} monotonically increases with ϕ, the underlying relationship between Le_{eff} and frequency becomes apparent. In addition, the observation of an increase in global frequency with increasing pressure and temperature is consistent with [2]. In other words, under higher initial pressures and temperatures, the cascade process of flame propagation occurs more frequently. A comprehensive amplitude database of hydrogen-air combustion is presented in Fig. 10. The amplitude B increases with the growth of ϕ and Le_{eff}. Furthermore, it has been observed that the parameter B exhibits a lesser degree of sensitivity to temperature variations but shows greater responsiveness to changes in pressure. The results demonstrated that B is dominated by thermal diffusion instability (characterized by Le_{eff}) and DL instability (highly susceptible to pressure). It is sensible to establish the empirical expressions for the experimentally obtained parameters (f, B) as a function of pressures and equivalence ratios:

$$f = 15400(0.144^{\phi})\left(\frac{P_i}{P_0}\right)^{0.544} \quad (R2 = 0.80) \tag{18}$$

$$B = 0.38(\phi^{1.3})\left(\frac{P_i}{P_0}\right)^{-1.07} \quad (R2 = 0.89) \tag{19}$$

Here, P_0 = 0.3 MPa. The fitting curves using Eqs. (18) and (19) are presented in Figs. 9 and 10, respectively, showing good agreement with experimental results.

4.6. Model validation

To validate the comprehensive correlation for pulsatory flame speed (Eq. (10), the experimental results of the hydrogen-air mixture derived from refs [2,27] are plotted in Fig. 11. The parameters in Eq.10, constant A, acceleration exponent α, pulsation frequency f, and pulsation

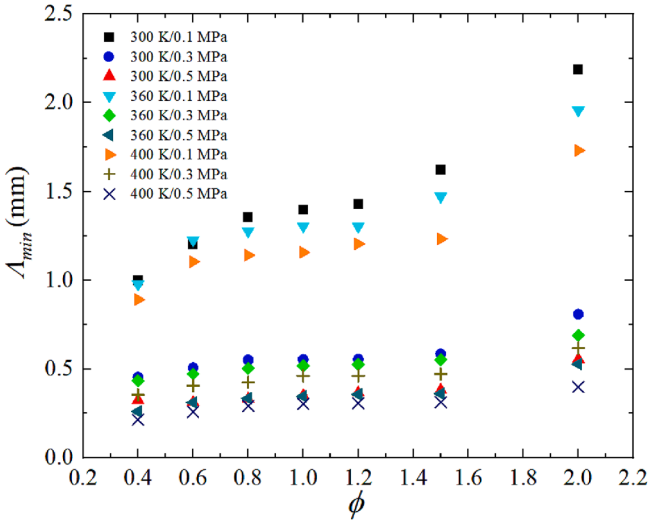

Fig. 12. Variations of mean cell size Λ_{min} against ϕ.

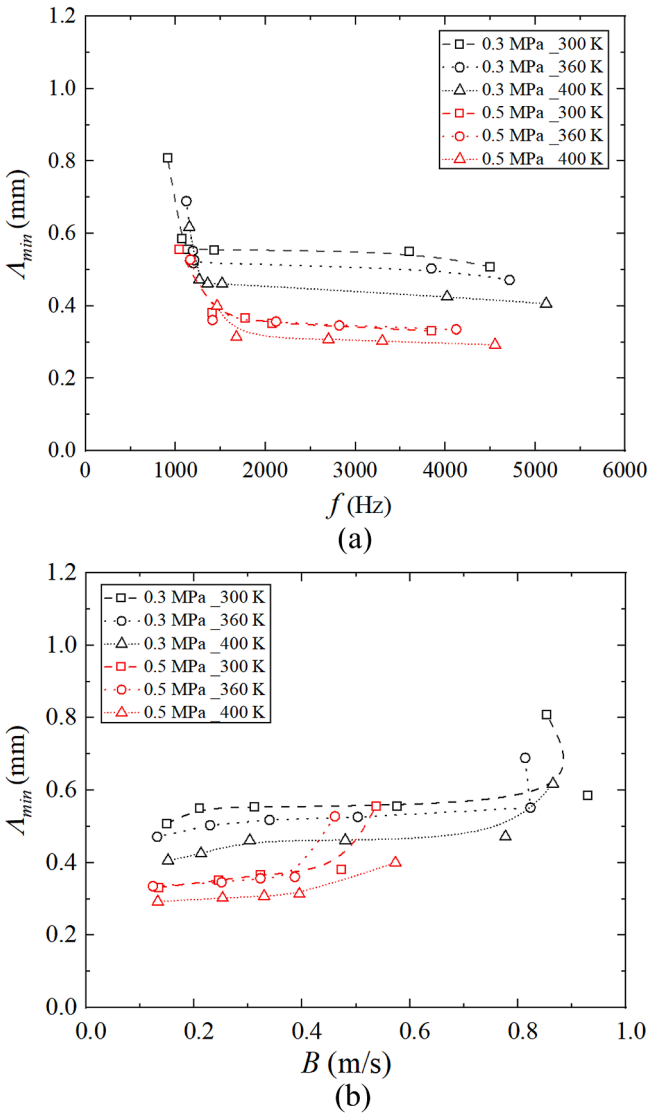

Fig. 13. (a) Λ_{min} *vs.* pulsation frequencies, *f*, (b) Λ_{min} *vs.* amplitudes, *B*.

amplitude *B*, have been previously presented and analyzed in the preceding sections. Based on this foundation, flame speed prediction curves after instability using Eq. (10) are added in Fig. 11, which are in good agreement with data from refs [2,27], notwithstanding minor disagreement. The discrepancy might be due to ignition energy, wall confinement, radiation, determination of phase differences λ etc. Moreover, Bauwens et al. [45] introduced a one-dimensional (1D) global pulsation model to account for the phenomenon of global pulsation resulting from the continuous growth and splitting of cells. The outcomes obtained from the 1D model are depicted in Fig. 11(b) for hydrogen-air flames at $\phi = 1.0$ and 1.1. The modeled results demonstrate a qualitatively similar trend to the experimental observations in terms of flame propagation, suggesting that the cell splitting and growth phenomena are adequately captured by the model. However, it should be noted that the frequency and amplitude predicted by the 1D model do not align well with the experimental data.

4.7. Mean cell size

As mentioned in Section 2.1, it is of interest to investigate the intrinsic relationship between cell size and the frequency of global pulsation. The theoretical mean cell sizes (Λ_{min}) of hydrogen-air mixture flames were calculated for each condition and plotted in Fig. 12. It is apparent that Λ_{min} increases with the increase of ϕ or Le_{eff}. Not surprisingly, increasing pressure results in smaller Λ_{min}. At high pressure, the reduced sensitivity to stretch rate results in greater susceptibility to instability [36] and subsequent smaller cell size. In accordance with experimental findings documented in reference [24], it has been observed that the cell radius of hydrogen-air flame reaches approximately 1.6 mm during the saturation stage under the specific conditions of $T_i = 383$ K, $P_i = 2$ bar, and $\phi = 0.4$. This measurement closely aligns with our theoretical calculations.

Consequently, Λ_{min} was plotted against the flame speed pulsation frequencies and amplitudes, shown in Fig. 13. What can be found in Fig. 13 (a) is that Λ_{min} decreases as frequency increases. This reveals that the great flame pulsation frequency is associated with small cell sizes on the flame surface, which is caused by the fast fission process due to strong thermal diffusion instability and hydrodynamic instability. In Fig. 13 (b), rising amplitude corresponds to the bigger cell size, further demonstrating the feasibility of the global pulsation assumption of the flame propagation speed.

Experimentally and macroscopically, it has been observed that hydrogen-air mixtures exhibit higher acceleration exponents when characterized by lower or negative Markstein numbers and Lewis numbers below unity. This behavior signifies a greater propensity for acceleration within this kind of mixture. Notably, intricate interactions between flames, local stretch, and differential diffusion at the microscale can manifest as substantial differences at the macroscale [43]. Furthermore, the turbulence-like structure observed in laminar unstable flames subsequent to instability indicates that both Darrieus-Landau (DL) and thermal diffusion (TD) instabilities may induce turbulence within a premixed flame brush or even propagate further through the gas flow. In the context of future fuel mixtures, it is particularly important to consider the susceptibility of light fuels, such as hydrogen, to instabilities or turbulence [46].

5. Conclusions

In the present investigation, the self-acceleration of unstable hydrogen-air flames were studied in a large fan-stirred vessel at various experimental conditions, providing empirical evaluations of the accelerated flame propagation regimes, which would improve the accuracy of modelling hydrogen flames. The key findings of the work are summarised in the following.

(1) The global pulsation features a cyclical strong and weak acceleration, or even a slowdown. A correlation for pulsating flame speed consisting of two terms (power-law growth of flame speed and sinusoidal pulsation) was updated and validated, and the parameters including constant *A*, acceleration exponent α, frequency *f*, amplitude, *B* have been derived using a least-square fitting method.

(2) The 1.5 exponent's assertion caused an overestimation in the flame speed for self-accelerating premixed hydrogen-air mixtures. The measured acceleration exponent in this study varies between 1.125 and 1.39 for premixed hydrogen-air flames over a wide range of initial conditions. A modified general expression of constant *A* taking stretch effects into account based on the acceleration exponent of 1.25. The similarity in acceleration exponents measured in small-scale laboratory explosions and those observed in large atmospheric conditions suggests that small-scale experiments can indeed serve as indicators or predictors of flame propagation in larger atmospheric settings. This implies that the insights and understanding acquired through the study of self-acceleration in small-scale laboratory explosions can be effectively utilized to enhance our comprehension and predictive capabilities regarding flame behavior on a larger scale.

(3) The empirical expressions for frequency and amplitude (*f*, *B*) were established as a function of pressures and equivalence

Table A1
Experimental data.

Temperature (K)	Pressure (MPa)	ϕ	α	σ_{sd}	A	σ_{sd}	B(m/s)	σ_{sd}	f(Hz)	σ_{sd}
300	0.1	0.4	1.3751	0.032	16.2	1.92	/	/	/	/
		0.6	1.3265	0.016	35.1	3.61	/	/	/	/
		0.8	1.307	0.023	73.2	4.01	/	/	/	/
		1	1.305	0.031	76.8	5.76	/	/	/	/
	0.3	0.4	1.272	0.013	10.3	0.58	/	/	/	/
		0.6	1.270	0.022	35.1	3.41	0.15	0.031	4500	104
		0.8	1.286	0.021	71.0	4.24	0.21	0.035	3600	89
		1	1.281	0.013	78.5	5.54	0.31	0.054	1430	76
		1.2	1.241	0.014	77.3	5.54	0.58	0.104	1128	65
		1.5	1.149	0.015	72.6	4.68	0.93	0.051	1070	18
		2	1.21	0.016	70.3	6.87	0.85	0.090	911	20
	0.5	0.4	1.312	0.006	9.4	0.29	/	/	/	/
		0.6	1.285	0.006	40.1	3.80	/	/	/	/
		0.8	1.300	0.008	94.0	4.58	0.14	0.033	3850	87
		1	1.289	0.008	108.3	5.65	0.25	0.041	2070	98
		1.2	1.266	0.012	91.0	6.29	0.32	0.073	1772	84
		1.5	1.220	0.015	71.3	7.04	0.47	0.074	1410	52
		2	1.170	0.015	52.3	4.53	0.54	0.055	1043	15
	0.7	0.4	1.322	0.010	8.2	0.60				
		0.6	1.312	0.015	44.5	4.32				
		0.8	1.309	0.010	96.1	4.90	0.12	0.009	4021	72
		1	1.292	0.010	119.1	6.17	0.16	0.018	3215	80
		1.2	1.271	0.011	109.5	6.61	0.20	0.070	2415	78
		1.5	1.232	0.011	75.1	7.56	0.24	0.094	1458	50
		2	1.191	0.019	64.6	4.84	0.33	0.081	1142	25
360	0.1	0.4	1.390	0.022	15.0	1.60	/	/	/	/
		0.6	1.335	0.015	33.0	2.43	/	/	/	/
		0.8	1.294	0.027	61.9	3.46	/	/	/	/
		1	1.286	0.009	73.3	3.61	/	/	/	/
	0.3	0.4	1.271	0.026	10.0	1.41	/	/	/	/
		0.6	1.268	0.014	36.5	3.24	0.13	0.025	4715	98
		0.8	1.262	0.025	64.3	5.46	0.23	0.036	3845	105
		1	1.249	0.016	62.5	5.54	0.34	0.042	1200	173
		1.2	1.227	0.014	63.3	5.68	0.50	0.076	1209	51
		1.5	1.140	0.015	73.9	7.55	0.82	0.046	1193	81
		2	1.180	0.016	73.1	5.50	0.81	0.083	1121	58
	0.5	0.4	1.270	0.032	8.8	0.93	/	/	/	/
		0.6	1.272	0.005	43.5	2.12	/	/	/	/
		0.8	1.286	0.009	90.7	4.23	0.12	0.018	4121	153
		1	1.275	0.009	94.3	5.45	0.25	0.077	2820	201
		1.2	1.236	0.012	82.5	6.05	0.32	0.026	2117	160
		1.5	1.177	0.015	69.3	6.11	0.39	0.006	1412	68
		2	1.187	0.015	47.7	5.06	0.46	0.01	1165	84
	0.7	0.4	1.301	0.009	6.86	0.68				
		0.6	1.287	0.010	54	4.31				
		0.8	1.287	0.018	91.3	6.20	0.10	0.060	4312	120
		1	1.288	0.012	106.5	7.49	0.14	0.013	3545	105
		1.2	1.251	0.009	100.3	7.493	0.18	0.070	2800	58
		1.5	1.212	0.014	80.3	6.64	0.22	0.094	1551	47
		2	1.202	0.009	61.1	6.97	0.31	0.094	1258	36
400	0.1	0.4	1.385	0.021	14.5	1.93	/	/	/	/
		0.6	1.322	0.017	37.0	2.77	/	/	/	/
		0.8	1.317	0.020	55.1	3.58	/	/	/	/
		1	1.281	0.030	70.8	4.15	/	/	/	/
	0.3	0.4	1.252	0.022	8.8	1.06	/	/	/	/
		0.6	1.233	0.014	32.1	3.14	0.15	0.011	5121	92
		0.8	1.228	0.011	59.3	4.75	0.21	0.025	4021	81
		1	1.225	0.010	61.0	5.48	0.30	0.074	1517	54
		1.2	1.177	0.013	62.2	7.78	0.48	0.071	1358	93
		1.5	1.125	0.021	67.1	4.24	0.78	0.047	1263	53
		2	1.160	0.014	61.1	9.19	0.87	0.050	1154	35
	0.5	0.4	1.268	0.012	9.0	0.67	/	/	/	/
		0.6	1.243	0.010	37.3	2.53	/	/	/	/
		0.8	1.251	0.010	74.2	6.24	0.13	0.01	4554	53
		1	1.243	0.013	91.0	5.29	0.25	0.018	3300	43
		1.2	1.211	0.014	81.7	6.53	0.33	0.071	2700	80
		1.5	1.175	0.020	67.0	5.73	0.40	0.094	1678	53
		2	1.170	0.016	46.3	3.48	0.57	0.042	1461	42
	0.7	0.4	1.271	0.014	7.84	0.72				
		0.6	1.261	0.010	40.15	3.31				
		0.8	1.261	0.019	78.51	6.30	0.10	0.090	4412	144
		1	1.258	0.013	100.10	6.08	0.12	0.011	3745	97
		1.2	1.223	0.016	89.62	6.59	0.17	0.090	2951	85
		1.5	1.181	0.020	71.54	6.52	0.20	0.094	1785	44
		2	1.192	0.018	60.27	4.06	0.31	0.071	1420	37

ratios. The comprehensive correlation of flame speed including pulsation was validated against previous work. It turns out that the newly proposed correlation is useful for predicting flame propagation speed after instability.

(4) The theoretical mean cell sizes of hydrogen-air mixture flames over a wide range of conditions are calculated. Strong thermal diffusion instability and hydrodynamic instability result in higher flame pulsation frequency, lower flame pulsation amplitude and smaller Λ_{min}.

CRediT authorship contribution statement

Yu Xie: Data curation, Formal analysis, Investigation, Methodology, Validation, Visualization, Writing – original draft. **Mohamed Elsayed Morsy:** . **Junfeng Yang:** Conceptualization, Formal analysis, Funding acquisition, Project administration, Resources, Supervision, Writing – original draft, Writing – review & editing.

Declaration of Competing Interest

The authors declare that they have no known competing financial interests or personal relationships that could have appeared to influence the work reported in this paper.

Data availability

Data will be made available on request.

Acknowledgements

Thanks are expressed to EPSRC (Grant No. EP/W002299/1) for the financial support. Yu Xie acknowledges the China Scholarship Council and University of Leeds for a joint PhD scholarship (CSC202008350141).

Appendix A1

Appendix A. Supplementary data

Supplementary data to this article can be found online at https://doi.org/10.1016/j.fuel.2023.129182.

References

[1] Wu F, Jomaas G, Law CK. An experimental investigation on self-acceleration of cellular spherical flames. Proc Combust Inst 2013;34(1):937–45.
[2] Huo J, Saha A, Ren Z, Law CK. Self-acceleration and global pulsation in hydrodynamically unstable expanding laminar flames. Combust Flame 2018;194:419–25.
[3] Gostintsev YA, Istratov AG, Shulenin YV. Self-similar propagation of a free turbulent flame in mixed gas mixtures. Combustion Explosion and Shock Waves 1988;24(5):563–9.
[4] D. Bradley, Instabilities and flame speeds in large-scale premixed gaseous explosions, Philosophical Transactions of the Royal Society of London. Series A: Mathematical, Physical and Engineering Sciences 357(1764) (1999) 3567-3581.
[5] Bradley D, Harper CM. The development of instabilities in laminar explosion flames. Combust Flame 1994;99(3–4):562–72.
[6] Bradley D, Sheppard CGW, Woolley R, Greenhalgh DA, Lockett RD. The development and structure of flame instabilities and cellularity at low Markstein numbers in explosions. Combust Flame 2000;122(1–2):195–209.
[7] Bradley D, Cresswell TM, Puttock JS. Flame acceleration due to flame-induced instabilities in large-scale explosions. Combust Flame 2001;124(4):551–9.
[8] Liang Z, Bauwens L. Cell structure and stability of detonations with a pressure-dependent chain-branching reaction rate model. Combust Theor Model 2005;9(1):93–112.
[9] Bauwens CR, Bergthorson JM, Dorofeev SB. Experimental study of spherical-flame acceleration mechanisms in large-scale propane–air flames. Proc Combust Inst 2015;35(2):2059–66.
[10] Kim WK, Mogi T, Kuwana K, Dobashi R. Self-similar propagation of expanding spherical flames in large scale gas explosions. Proc Combust Inst 2015;35(2):2051–8.
[11] Cai X, Wang J, Zhao H, Zhang M, Huang Z. Flame morphology and self-acceleration of syngas spherically expanding flames. Int J Hydrogen Energy 2018;43(36):17531–41.
[12] Cai X, Wang J, Bian Z, Zhao H, Dai H, Huang Z. On transition to self-similar acceleration of spherically expanding flames with cellular instabilities. Combust Flame 2020;215:364–75.
[13] Xie Y, Wang J, Cai X, Huang Z. Self-acceleration of cellular flames and laminar flame speed of syngas/air mixtures at elevated pressures. Int J Hydrogen Energy 2016;41(40):18250–8.
[14] Li Y, Bi M, Gao W, Cong H, Li B. Self-acceleration and self-similarity of hydrogen-methane-air flame at elevated pressure. Combust Sci Technol 2021;193(6):1005–21.
[15] C.D. Lind, J.C. Whitson, Explosion hazards associated with spills of large quantities of hazardous materials. Phase II. Final report (No. AD-A-047585). Naval Weapons Center, China Lake, Calif.(USA) (1977).
[16] Gostintsev YA, Istratov AG, Kidin NI, Fortov VE. Autoturbulization of gas flames: theoretical treatment. High Temp 1999;37(4):603–7.
[17] Gostintsev YA, Fortov VE, Shatskikh YV. Self-similar propagation law and fractal structure of the surface of a free expanding turbulent spherical flame. Dokl Phys Chem 2004;397(1):141–4.
[18] Kwon OC, Rozenchan G, Law CK. Cellular instabilities and self-acceleration of outwardly propagating spherical flames. Proc Combust Inst 2002;29(2):1775–83.
[19] Haq MZ. Correlations for the onset of instabilities of spherical laminar premixed flames. J Heat Transfer 2005;127:1410–5.
[20] Kim W, Sato Y, Johzaki T, Endo T, Shimokuri D, Miyoshi A. Experimental study on self-acceleration in expanding spherical hydrogen-air flames. Int J Hydrogen Energy 2018;43(27):12556–64.
[21] Kim W, Namba T, Johzaki T, Endo T. Self-similar propagation of spherically expanding flames in lean hydrogen-air mixtures. Int J Hydrogen Energy 2020;45(46):25608–14.
[22] Yang S, Saha A, Wu F, Law CK. Morphology and self-acceleration of expanding laminar flames with flame-front cellular instabilities. Combust Flame 2016;171:112–8.
[23] Okafor EC, Nagano Y, Kitagawa T. Experimental and theoretical analysis of cellular instability in lean H_2-CH_4-air flames at elevated pressures. Int J Hydrogen Energy 2016;41(15):6581–92.
[24] Bauwens CRL, Bergthorson JM, Dorofeev SB. Experimental investigation of spherical-flame acceleration in lean hydrogen-air mixtures. Int J Hydrogen Energy 2017;42(11):7691–7.
[25] Huang S, Huang R, Zhang Y, Zhou P, Wang Z, Yin Z. Relationship between cellular morphology and self-acceleration in lean hydrogen-air expanding flames. Int J Hydrogen Energy 2019;44(59):31531–43.
[26] Zhao H, Li G, Wang J, Yuan C, Huang Z. Effects of density ratio and differential diffusion on flame accelerative propagation of H2/O2/N2 mixtures. Int J Hydrogen Energy 2023;48(24):9071–81.
[27] Huo J, Saha A, Shu T, Ren Z, Law CK. Self-acceleration and global pulsation in expanding laminar H_2–O_2–N_2 flames. Phys Rev Fluids 2019;4(4):043201.
[28] Liu Z, Unni VR, Chaudhuri S, Sui R, Law CK, Saha A. Self-turbulization in cellularly unstable laminar flames. J Fluid Mech 2021;917.
[29] Filyand L, Sivashinsky GI, Frankel ML. On self-acceleration of outward propagating wrinkled flames. Phys D: Nonlinear Phenom 1994;72(1-2):110–8.
[30] Xin YX, Yoo CS, Chen JH, Law CK. A DNS study of self-accelerating cylindrical hydrogen–air flames with detailed chemistry. Proc Combust Inst 2015;35(1):753–60.
[31] Al-Shahrany AS, Bradley D, Lawes M, Liu K, Woolley R. Darrieus-Landau and thermo-acoustic instabilities in closed vessel explosions. Combust Sci Technol 2006;178(10–11):1771–802.
[32] Goulier J, Comandini A, Halter F, Chaumeix N. Experimental study on turbulent expanding flames of lean hydrogen/air mixtures. Proc Combust Inst 2017;36(2):2823–32.
[33] Addabbo R, Bechtold JK, Matalon M. Wrinkling of spherically expanding flames. Proc Combust Inst 2002;29(2):1527–35.
[34] Göttgens J, Mauss F, Peters N. Analytic approximations of burning velocities and flame thicknesses of lean hydrogen, methane, ethylene, ethane, acetylene, and propane flames. Symp (Int) Combust 1992;24(1):129–35.
[35] C. Morley, Gaseq: a chemical equilibrium program for Windows. Ver. 0.79. 2005.
[36] Xie Y, Morsy ME, Li J, Yang J. Intrinsic cellular instabilities of hydrogen laminar outwardly propagating spherical flames. Fuel 2022;327:125149.
[37] Xie Y, Li J, Yang J, Cracknell R. Laminar burning velocity blending laws using particle imaging velocimetry. Applications in Energy and Combustion Science 2023;13:100114.
[38] Xie Y, Lu A, Li J, Yang J, Zhang C, Morsy ME. Laminar burning characteristics of coal-based naphtha. Combust Flame 2023;249:112625.
[39] Kasthuri P, Pawar SA, Gejji R, Anderson W, Sujith RI. Coupled interaction between acoustics and unsteady flame dynamics during the transition to thermoacoustic instability in a multi-element rocket combustor. Combust Flame 2022;240:112047.
[40] Aspden AJ, Day MS, Bell JB. Bell, Three-dimensional direct numerical simulation of turbulent lean premixed methane combustion with detailed kinetics. Combust Flame 2016;166:266–83.
[41] Aspden AJ, Bell JB, Day MS, Egolfopoulos FN. Turbulence–flame interactions in lean premixed dodecane flames. Proc Combust Inst 2017;36(2):2005–16.
[42] Aspden AJ. A numerical study of diffusive effects in turbulent lean premixed hydrogen flames. Proc Combust Inst 2017;36(2):1997–2004.

[43] Hochgreb S. How fast can we burn, 2.0. Proc Combust Inst 2023;39(2):2077–105.
[44] M.A. Liberman, M.F. Ivanov, O.E. Peil, D.M. Valiev, L.E. Eriksson, Self-acceleration and fractal structure of outward freely propagating flames, Physics of Fluids 16(7) (2004) 2476-2482.
[45] Bauwens CRL, Bergthorson JM, Dorofeev SB. Modeling the formation and growth of instabilities during spherical flame propagation. Proc Combust Inst 2019;37(3):3669–76.
[46] Ahmed P, Thorne B, Lawes M, Hochgreb S, Nivarti GV, Cant RS. Three dimensional measurements of surface areas and burning velocities of turbulent spherical flames. Combust Flame 2021;233:111586.